Indian Journal of Pure & Applied Physics
Vol. 58, May 2020, pp. 331-335

# Relative emergence of fission and quasi-fission in Z=116 superheavy nucleus

Gurjit Kaur* & Manoj K Sharma

School of Physics and Materials Science, Thapar Institute of Engineering and Technology, Patiala 147 004, India

*Received 23 March 2020*

The fusion and subsequent decay analysis of Z=116 superheavy nucleus formed via $^{48}Ca+^{248}Cm\rightarrow^{296}Lv^{*}$, $^{50}Ti+^{244}Pu\rightarrow^{294}Lv^{*}$,and $^{58}Fe+^{232}Th\rightarrow^{290}Lv^{*}$ reactions is carried out using extended ℓ-summed Wong model and dynamical cluster decay model (DCM), respectively. First of all, the experimentally available fusion-fission (A/2±20) data is adequately addressed for $^{296}Lv^{*}$ and $^{294}Lv^{*}$ superheavy nuclei using extended ℓ-summed Wong model and the predictions are made for fusion-fission excitation function of $^{290}Lv^{*}$ nucleus. It is observed that with decrease in mass-asymmetry (η), the contribution of fusion-fission component decreases. This drop is steeper for $^{50}Ti$ to $^{58}Fe$ as compared to that for $^{48}Ca$ to $^{50}Ti$. The calculated values of compound nucleus formation probability ($P_{CN}$) are highest for $^{48}Ca$ followed by $^{50}Ti$ and $^{58}Fe$. Finally, the mass distribution of decay fragments is studied for $^{296}Lv^{*}$, $^{294}Lv^{*}$, and $^{290}Lv^{*}$ nuclei using DCM at near barrier energies. A valley in $A_{CN}/2$ region results in asymmetric mass distribution for $^{296}Lv^{*}$ which becomes relatively symmetric for the lighter isotope $^{290}Lv^{*}$.

**Keywords:** Heavy ion induced reactions, Fusion-fission, Superheavy nuclei, Mass and potential distribution

## 1 Introduction

The interpretation of fusion-fission dynamics of superheavy nuclei attracts huge attention due to the motivation of obtaining utmost conditions for the synthesis of stable nuclei in this extreme mass region. In hot and cold fusion reactions leading to the synthesis of superheavy nuclei, the quasi-fission is the dominant decay mode which hinders the emergence of stable compound nucleus. Therefore, the knowledge of fission characteristics like ratio of fission and quasi-fission contribution, entrance channel mass-asymmetry, excitation energy, kinetic energy of fragments *etc* are of great interest to the nuclear physicists working in the area of superheavy nuclei (SHN)[1-3]. The success in the synthesis of Z=112-118 produced in $^{48}Ca$-induced reactions advocate the existence of island of stability near proton magic Z=120, 126 and N=184[4,5]. Continuous efforts are being made to reach this stable regime where superheavy nuclei with sufficient half-lives be produced.

It is well known that, the production of superheavy elements with Z>118 requires projectile heavier than $^{48}Ca$ such as $^{50}Ti$ and $^{58}Fe$ because heaviest available stable target so far is $^{249}Cf$. Also, the decrease in mass-asymmetry of entrance channel, affects the relative contribution of fusion-fission (FF) and quasi-fission (QF) events towards capture cross-sections. Therefore, certain features of FF and QF processes in term of mass distribution of fragments, width of mass-distribution, and relative contribution towards total cross-sections are of great interest, which in turn may facilitate to optimize the conditions for the synthesis of stable superheavy nuclei.

In view of this, present study is devoted to scrutinize the isotopes of Z=116 formed via different entrance channels i.e. $^{48}Ca+^{248}Cm\rightarrow^{296}Lv^{*}$, $^{50}Ti+^{244}Pu\rightarrow^{294}Lv^{*}$, and $^{58}Fe+^{232}Th\rightarrow^{290}Lv^{*}$. The decay dynamics of $^{48}Ca+^{248}Cm\rightarrow^{296}Lv^{*}$ reaction was studied earlier within the dynamical cluster decay model (DCM)[6,7] within the framework of dynamical cluster decay model (DCM). As an extension, the present work is carried out to study the entrance channel effects of Z=116 superheavy nucleus. The experimentally[8,9] available fusion-fission cross-sections (A/2±20) are calculated at energies near and above the Coulomb barrier using extended ℓ-summed Wong model[10,11] which are in decent agreement with the experimental data. Further, the cross-sections are predicted for $^{58}Fe+^{232}Th\rightarrow^{290}Lv^{*}$ reaction using same methodology. Finally, the decay analysis of $^{296}Lv^{*}$, $^{294}Lv^{*}$, and $^{290}Lv^{*}$ nuclei is carried out using the dynamical cluster decay model (DCM)[12,13]. The fragmentation and preformation mass yield of aforesaid isotopes are studied in context to explore the fission dynamics.

*Corresponding author (E-mail: gurjitsaini2505@gmail.com)

## 2 Methodology

### 2.1 ℓ-Summed Wong model

The capture cross sections in term of angular-momentum (ℓ) partial waves for two deformed and oriented nuclei are given as:

$$\sigma_{Cap}(E_{c.m.},\theta_i)=\frac{\pi}{k^2}\sum_{\ell=0}^{\ell_{\max}}(2\ell+1)P_\ell;k=\sqrt{\frac{2\mu E_{c.m.}}{\hbar^2}} \quad \ldots (1)$$

with $\ell_{\max}=\frac{R_a\sqrt{2\mu[E_{c.m.}-V(R_a,\ell=0)}}{\hbar}$ ,

here μ is the reduced mass and $P_\ell$ is the transmission coefficient which describe the penetrability across the barrier using Hill Wheeler approximation[14] as:

$$P_\ell=\left[1+\exp\left(\frac{2\pi(V_B^\ell-E_{c.m.})}{\hbar\omega_\ell}\right)\right]^{-1} \quad \ldots (2)$$

Here barrier parameters $V_B^\ell$, $\omega_\ell$, and $R_B^\ell$ are calculated at different values of angular momentum (ℓ) unlike Wong model in which these are calculated at ℓ=0. The cross-sections are calculated for each orientation to give final capture cross-section as:

$$\sigma_{Cap}(E_{c.m.},\theta_i)=\int_{\theta_i=0}^{\pi/2}\sigma(E_{c.m.},\theta_i)\sin\theta_1 d\theta_1\sin\theta_2 d\theta_2 \quad \ldots (3)$$

As the fusion cross-sections contribute only a part to capture events in case of superheavy nuclei. Therefore fusion cross-sections can be determined by relation $\sigma_{fusion}=\sigma_{Cap}P_{CN}$ which is written as:

$$\sigma_{fusion}(E_{c.m.},\theta_i)=\sum_{\ell=0}^{\ell_{\max}}(2\ell+1)P_\ell P_{CN} \quad \ldots (4)$$

The evaporation residue cross-sections for these nuclei are very small in comparison to fusion-fission so one can assume $\sigma_{fusion}\approx\sigma_{fusion-fission}$. The compound nucleus formation probability ($P_{CN}$) used in above equation is defined as[8,15]:

$$P_{CN}(E^*)=\frac{P_{CN}^0}{1+\exp\left[\left(E_B^*-E_{CN}^*\right)/4\right]} \quad \ldots (5)$$

With "asymptotic fusion probability" as:

$$P_{CN}^0=\frac{1}{1+\exp(x_m-0.721)/0.0226} \quad \ldots (6)$$

### 2.2 Dynamical cluster-decay model

Based on the quantum mechanical fragmentation theory[16,17] (QMFT), the dynamical cluster-decay model[12,13] (DCM) employs the collective coordinates of mass (and charge asymmetries) $\eta_A=(A_1-A_2)/(A_1+A_2)$ (and $\eta_Z=(Z_1-Z_2)/(Z_1+Z_2)$), the relative separation R, the multipole deformations $\beta_{\lambda i}$(λ=2, 3, 4; $i$=1, 2) of decaying fragments. In terms of these coordinates, for ℓ-partial waves, the decay cross-section is as:

$$\sigma=\frac{\pi}{k^2}\sum_{\ell=0}^{\ell_{\max}}(2\ell+1)P_0P \quad \ldots (7)$$

Using this equation, the fission cross-sections are defined as:

$$\sigma_{(A/2)\pm20}=2\sum_{A_2=(\frac{A}{2})-20}^{A/2}\sigma(A_1,A_2) \quad \ldots (8)$$

where $\mu=mA_1A_2/(A_1+A_2)$ is the reduced mass, and maximum angular momentum ($\ell_{\max}$) fixed where the cross-sections of light particles become negligibly small. $P_0$, the fragment's preformation probability, refers to $\eta$-motion, contains structure information of compound nucleus (CN), and is calculated by solving stationary Schrodinger equation in $\eta$-coordinate, at fixed $R=R_a$(the first turning point),

$$P_0=\left|\psi(\eta(A_i))\right|^2\sqrt{B_{\eta\eta}}\frac{2}{A_{CN}} \quad \ldots (9)$$

$B_{\eta\eta}$ are the smooth hydrodynamical mass parameters, representing the kinetic energy part of Hamiltonian[18]. The fragmentation potential V(R,η,T), calculated at fixed $R=R_a$, is the sum of liquid drop energy $V_{LDM}$, shell corrections ( δU), Coulomb ($V_C$), centrifugal ($V_\ell$) and proximity ($V_P$) potentials, as:

$$V_R(\eta,T) = \sum_{i=1}^{2} V_{LDM}\ (A_i,Z_i,T) + \sum_{i=1}^{2} \delta U_i \exp(-T^2/T_0^2) + V_C(A_i,Z_i,\beta_{\lambda i},\theta_i,T) + V_P(A_i,Z_i,\beta_{\lambda i},\theta_i,T) + V_\ell(A_i,Z_i,\beta_{\lambda i},\theta_i,T) \quad \ldots (10)$$

for details see Ref.[19]. The penetrability P in Eq. (1) refers to R-motion, and is calculated using Wenzel-Kramers-Brillouin (WKB) integral.

## 3 Results and Discussion

This section describes the calculations and results in view of ℓ-summed Wong model and dynamical cluster decay model for Z=116 superheavy nucleus formed in different entrance channels i.e. $^{48}$Ca+$^{248}$Cm→$^{296}$Lv$^*$(η=0.67), $^{50}$Ti+$^{244}$Pu→$^{294}$Lv$^*$(η=0.65), and $^{58}$Fe+$^{232}$Th→$^{290}$Lv$^*$(η=0.60). The dynamics of Z=116 superheavy nucleus is analyzed by introducing two set of calculations. In the first set, the fusion mechanism is addressed using ℓ-summed Wong model. The experimentally available fusion-fission cross-sections ($\sigma_{A/2\pm20}$) for $^{296}$Lv$^*$ and $^{294}$Lv$^*$ are addressed within this methodology at energies near and above the Coulomb barrier. Following this, the decay dynamics of aforesaid nuclei is addressed using dynamical cluster decay model (DCM). In the first set, Fig. 1 shows the variation of fusion-fission cross-sections ($\sigma_{A/2\pm20}$) with excitation energy ($E^*_{CN}$). The experimentally available data for $^{48}$Ca+$^{248}$Cm→$^{296}$Lv$^*$ and $^{50}$Ti+$^{244}$Pu→$^{294}$Lv$^*$ reactions is addressed using ℓ-summed Wong model. The theoretical cross-sections are in decent agreement with the available experimental data. As the main motive of the present work is to study the entrance channel effects, hence the fusion-fission excitation function is calculated for $^{58}$Fe+$^{232}$Th→$^{290}$Lv$^*$ reaction which can be verified via future experiments. Among the studied reactions, the cross-sections are observed to be least for $^{58}$Fe–induced reactions. It is evident from Fig.1 that the decrease in mass-asymmetry influences the contribution of fission to a great extent and hence the cross-sections decreases accordingly. At near barrier energies, the fusion-fission cross-sections drop at a relatively faster pace while shifting from $^{50}$Ti to $^{58}$Fe than that for $^{48}$Ca to $^{50}$Ti.

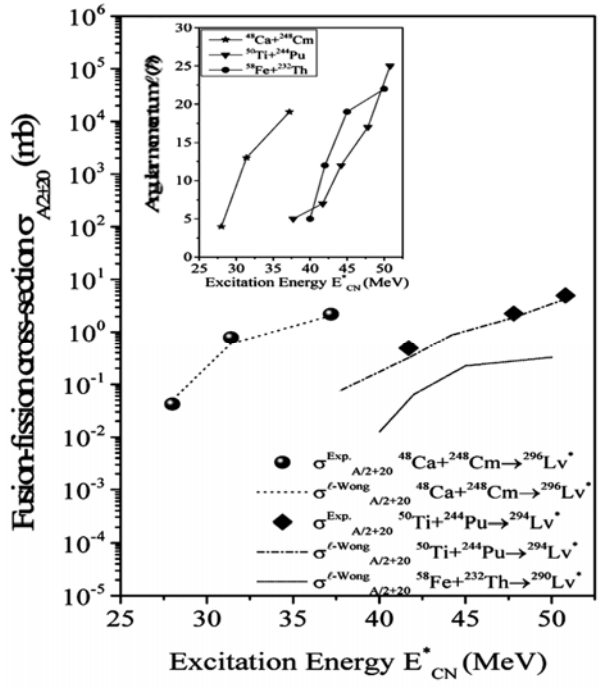


Fig.1 – Variation of fusion-fission cross-sections ($\sigma_{A/2\pm20}$) as a function of excitation energy ($E^*_{CN}$) for Z=116 superheavy nucleus formed in $^{48}$Ca+$^{248}$Cm→$^{296}$Lv$^*$, $^{50}$Ti+$^{244}$Pu→$^{294}$Lv$^*$, and $^{58}$Fe+$^{232}$Th→$^{290}$Lv$^*$ hot fusion reactions.

To understand the fusion dynamics better, the compound nucleus formation probability ($P_{CN}$) is plotted as a function of excitation energy ($E^*_{CN}$) for aforesaid reactions in Fig. 2. The value of $P_{CN}$ increases with increase in excitation energy. The magnitude of $P_{CN}$ (calculated using Eq. (5)) is highest for $^{48}$Ca+$^{248}$Cm→$^{296}$Lv$^*$ reaction and least for $^{58}$Fe+$^{232}$Th→$^{290}$Lv$^*$ which means that, the $P_{CN}$ values of $^{50}$Ti+$^{244}$Pu→$^{294}$Lv$^*$ are in between the above two reactions. Interestingly, the difference of compound nucleus formation probability between $^{48}$Ca and $^{50}$Ti

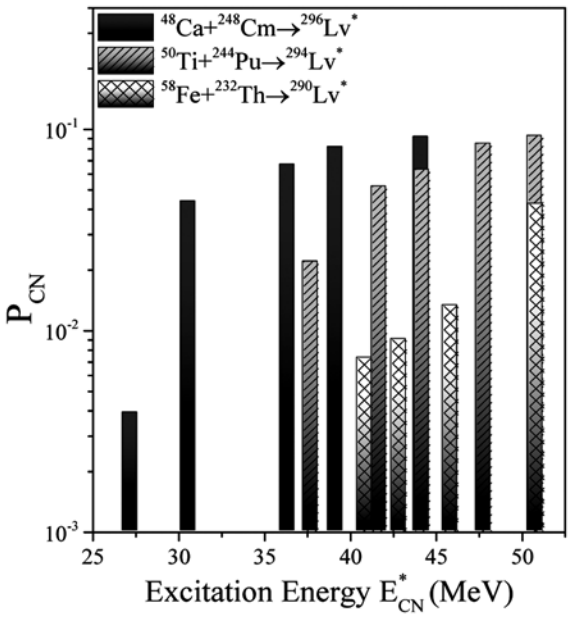


Fig. 2 – Compound nucleus formation probability ($P_{CN}$) plotted as a function of excitation energy ($E^*_{CN}$) for $^{296}$Lv$^*$, $^{294}$Lv$^*$, and $^{290}$Lv$^*$ superheavy isotopes.

is smaller as compare to that for $^{48}$Ca and $^{58}$Fe. This suggests that after $^{48}$Ca, $^{50}$Ti projectile gives an alternative option to synthesize superheavy nuclei. The decay dynamics of aforesaid reactions are further studied using dynamical cluster decay model (DCM).

The $\sigma_{A/2\pm20}$ cross-sections are calculated at energies close to the Coulomb barrier. The calculated cross-sections along with neck-length parameter ($\Delta$R) are shown in Fig. 3 as a function of mass of the composite system. The fission cross-sections are in decent agreement with the experimental data for $^{296}$Lv$^*$ and $^{294}$Lv$^*$ and predicted values of $^{290}$Lv$^*$ nucleus. From this figure it can be manifested that at energies near the Coulomb barrier, with increase in mass of the composite system, cross-sections increases. On the contrary, the neck-length parameter ($\Delta$R) decreases. It is relevant to mention here that $\Delta$R allows us to optimize the barrier parameters relative to experimental data which is further helpful in the analysis of decay dynamics.

Next, to explore the fission distribution, the preformation probability of symmetric fission fragments is plotted in Fig. 4 (a-c) for reactions induced via $^{48}$Ca, $^{50}$Ti, and $^{58}$Fe projectiles at energies near the Coulomb barrier. It can be clearly seen from this figure that at transition from $^{48}$Ca to $^{58}$Fe, the shape of fission fragment mass distribution changes significantly. The two humped mass distributions are observed for all the studied reactions with peaks of fragments around doubly magic tin (Sn, $M_L$~134u) in the symmetric region of the fragments (A/2±20). The mass distribution is highly asymmetric for the reaction with $^{48}$Ca-projectile due to the appearance of a valley in A/2 region. But for the reaction with $^{58}$Fe, this valley disappears and a relatively symmetric structure is obtained. This might be due to the damping of shell effects with increase in temperature. At higher temperature (and hence energy), shell effects will be less effective and the mass drift toward symmetry will eventually saturate the fragments into symmetric distribution. To underline the impact of entrance channel further, Fig. 5 is plotted which shows the enlarged view of fragmentation potential for $^{48}$Ca+$^{248}$Cm, $^{50}$Ti+$^{244}$Pu,and $^{58}$Fe+$^{232}$Th reactions in the region of QF. From this figure, one can observe that the quasi-fission valleys are observed across different isotopes of Lead (Pb). For lighter mass of Z=116 i.e. $^{290}$Lv$^*$, a lighter isotopes of Pb ($^{208}$Pb) is observed which increase in mass ($^{212}$Pb) for heavier isotope ($^{296}$Lv$^*$). The width of potential curve also changes for different reactions. A broader potential

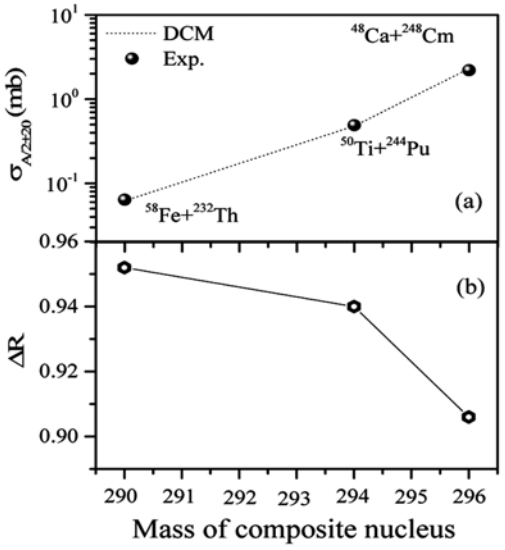


Fig. 3 – (a) Fusion-fission cross-sections ($\sigma_{A/2\pm20}$) and (b) neck-length parameter ($\Delta$R) plotted as a function of mass of composite system at energies close to the Coulomb barrier using DCM.

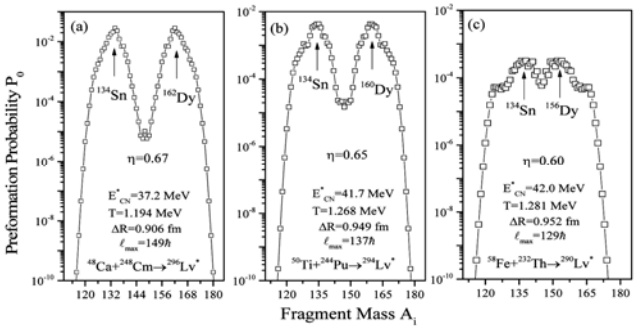


Fig. 4 – Preformation yield $P_0$ as a function of fragment mass $A_i$ in symmetric region (A/2±20) for (a) $^{48}$Ca+$^{248}$Cm→$^{296}$Lv$^*$,(b) $^{50}$Ti+$^{244}$Pu→$^{294}$Lv$^*$, and (c) $^{58}$Fe+$^{232}$Th→$^{290}$Lv$^*$ hot fusion reactions at energies close to the Coulomb barrier.

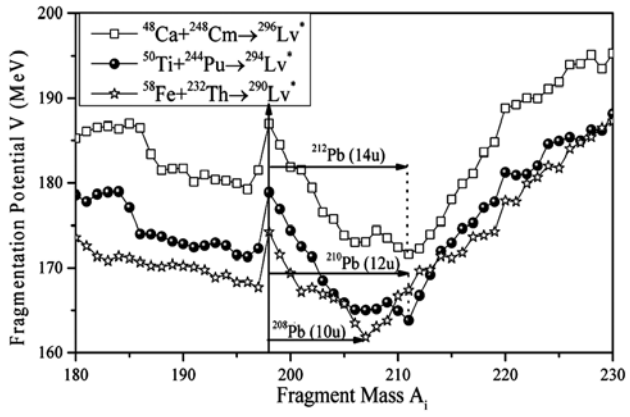


Fig. 5 – Enlarged view of fragmentation potential for quasi-fission region near Lead (Pb) with fragment mass $A_i$ at near barrier energies.

curve with width 14u is observed for $^{296}$Lv$^*$ (across $^{212}$Pb) which is relatively sharp with width 10u for

$^{290}Lv^{*}$ (across $^{208}Pb$). Larger the mass width, wider is the potential well and hence larger mass flow occurs toward symmetric region which results in relatively smaller contribution of QF and vice-versa. This means that the contribution of QF events is maximum for $^{58}Fe+^{232}Th\rightarrow^{290}Lv^{*}$ following $^{50}Ti+^{244}Pu\rightarrow^{294}Lv^{*}$ and $^{48}Ca+^{248}Cm\rightarrow^{296}Lv^{*}$ reaction.

## 4 Conclusions

Based on the calculations and discussion, we draw the following conclusions:

(i) After $^{48}Ca$, $^{50}Ti$ seems a probable option to synthesize superheavy nuclei.

(ii) The mass distribution is highly asymmetric for $^{48}Ca+^{248}Cm\rightarrow^{296}Lv^{*}$ reaction which turn out to be symmetric on moving toward $^{58}Fe+^{232}Th\rightarrow^{290}Lv^{*}$. This means that with decrease in mass-asymmetry the mass drifts toward symmetric region.

(iii) The asymmetric QF valley is sharp for $^{58}Fe$ channel and is relatively broader for $^{48}Ca$ case.

## Acknowledgement

The financial support from the UGC-DAE Consortium for Scientific Research, F.No. UGC-DAE-CSRKC/CRS/19/NP09/0920 and INSPIRE-fellowship (grant no. DST/INSPIRE/03/2015/000199) is gratefully acknowledged.

## References

1 Itkis M G, Vardaci E, Itkis I M, Knyazheva G N & Kozulina E M, *Nucl Phys A*, 944 (2015) 204.
2 Hofmann S, Heßberger F P, Ackermann D, Munzenberg G, Antalic S, Cagarda P, Kindler B, Kojouharova J, Leino M, Lommel B, Mann R, Popeko A G, Reshitko S, Saro S, Uusitalo J & Yeremin A V, *Eur Phys J A*, 14 (2002) 147.
3 Oganessian Y T, *Pure Appl Chem*, 76 (2004) 1715.
4 Oganessian Y T, *J Phys G; Nucl Part Phys*, 34 (2007) R165.
5 Oganessian Y T & Utyonkov V K, *Nucl Phys A*, 944 (2015) 62.
6 Sandhu K & Sharma M K, *AIP Conf Proc*, 1524 (2013) 123.
7 Kaur G, Sandhu K & Sharma M K, *Phys Rev C*, 94 (2016) 014615.
8 Itkis M G, Bogachev A A, Itkis I M, Kliman J, Knyazheva G N, Kondratiev N A, Kozulin E M, Krupa L, Oganessian Y T, Pokrovsky I V, Prokhorova E V & Rusanov A Y, *Nucl Phys A*, 787 (2007) 150.
9 Kozulin E M, Knyazheva G N, Itkis I M, Itkis M G, Bogachev A A, Chernysheva E V, and Krupa L, Hanappe F, Dorvaux O, Stuttge L, Trzaska W H, Schmitt C & Chubarian G, *Phys Rev C*, 90 (2014) 054608.
10 Wong C Y, *Phys Rev Lett*, 31 (1973) 766.
11 Kumar R, Bansal M, Arun S K & Gupta R K, *Phys Rev C*, 80 (2009) 034618.
12 Kaur G & Sharma M K, *Nucl Phys A*, 990 (2019) 79.
13 Sandhu K, Sharma M K & Gupta R K, *Phys Rev C*, 86 (2012) 064611.
14 Hill D L & Wheeler J A, *Phys Rev*, 89 (1953) 1102.
15 Zagrebaev V I & Greiner W, *Nucl Phys A*, 944 (2015) 257.
16 Maruhn J & Greiner W, *Phys Rev Lett*, 32 (1974) 548.
17 Gupta R K, Scheid W & Greiner W, *Phys Rev Lett*, 35 (1975) 353.
18 Kröger H & Scheid W, *J Phys G*, 6 (1980) L85.
19 Gupta R K, Singh N & Manhas M, *Phys Rev C*, 70 (2004) 034608.